ADVANCED MATERIALS
www.advmat.de

Perovskite Quantum Dots with Near Unity Solution and Neat-Film Photoluminescent Quantum Yield by Novel Spray Synthesis

*Shu-Wen Dai, Bo-Wei Hsu, Chien-Yu Chen, Chia-An Lee, Hsiao-Yun Liu, Hsiao-Fang Wang, Yu-Ching Huang, Tien-Lin Wu, Arumugam Manikandan, Rong-Ming Ho, Cheng-Si Tsao, Chien-Hong Cheng, Yu-Lun Chueh, and Hao-Wu Lin**

In this study, a novel perovskite quantum dot (QD) spray-synthesis method is developed by combining traditional perovskite QD synthesis with the technique of spray pyrolysis. By utilizing this new technique, the synthesis of cubic-shaped perovskite QDs with a homogeneous size of 14 nm is demonstrated, which shows an unprecedented stable absolute photoluminescence quantum yield ≈100% in the solution and even in the solid-state neat film. The highly emissive thin films are integrated with light emission devices (LEDs) and organic light emission displays (OLEDs). The color conversion type QD-LED (ccQD-LED) hybrid devices exhibit an extremely saturated green emission, excellent external quantum efficiency of 28.1%, power efficiency of 121 lm W^{-1}, and extraordinary forward-direction luminescence of 8 500 000 cd m^{-2}. The conceptual ccQD-OLED hybrid display also successfully demonstrates high-definition still images and moving pictures with a 119% National Television System Committee 1931 color gamut and 123% Digital Cinema Initiatives-P3 color gamut. These very-stable, ultra-bright perovskite QDs have the properties necessary for a variety of useful applications in optoelectronics.

Organometallic lead halide perovskites have received great attention recently due to their potential application in the fabrication of very efficient optoelectronic and electronic devices, including solar cells,[1–3] light emission devices (LEDs),[4–13] lasers,[14] transistors,[15,16] and memories.[17,18] Among them, nanosize perovskite quantum dots (QDs) with confined excitonic structures were found to show promising photoluminescent (PL) quantum yields (PLQYs) and widely tunable emission wavelength ranges.[19–22] The synthesis of these organometallic lead halide perovskite QDs usually involves of the injection of good-solvent-dissolved organic halides and lead halides into poor solvents. The perovskite QDs then nanocrystallize in the poor solvents. However, the QDs formed with this method usually possess irregularly spherical shapes unlike their inorganic cesium (Cs)–lead halide counterparts that usually exhibit a perfect cubic shape.[19,21,23,24] Moreover, although these perovskite quantum dots display good PLQYs up to 70–80% in the solution form, they usually suffer from poor PLQY (<30–40%) in the neat films due to severe quenching.[24]

High-temperature spray pyrolysis is one of the widely used techniques to fabricate nanoparticles, especially nanosize oxide particles.[25,26] The micrometer-size droplets with the precursors react on the heated surface and form the nanosize products after solvent evaporation. In this paper, we report a new perovskite QD spray-synthesis method by utilizing a combination of the traditional perovskite QD synthesis in conjunction with the popular technique of spray pyrolysis. The resulting organometallic lead halide perovskite QDs intriguingly showed a highly crystallized cubic shape with a 100% absolute PLQY in the solution form. Furthermore, negligible quenching was found in the neat QD films, which showed a saturated 526 nm green emission with a full-width-at-half-maximum (FWHM) wavelength width of 20 nm and a high absolute PLQY also up to 100%. The highly emissive green QD films were employed as a color conversion layer and were pumped with ultraviolet (UV) LEDs. The green-emission devices showed very high external quantum efficiency (EQE) up to 28.1% and extraordinary maximum forward

S.-W. Dai, B.-W. Hsu, C.-Y. Chen, C.-A. Lee, H.-Y. Liu, A. Manikandan, Prof. Y.-L. Chueh, Prof. H.-W. Lin
Department of Materials Science and Engineering
National Tsing Hua University
Hsinchu 30013, Taiwan
E-mail: hwlin@mx.nthu.edu.tw
Dr. H.-F. Wang, Prof. R.-M. Ho
Department of Chemical Engineering
National Tsing Hua University
Hsinchu 30013, Taiwan
Dr. Y.-C. Huang, Prof. C.-S. Tsao
Institute of Nuclear Energy Research
Taoyuan 32546, Taiwan
Prof. C.-S. Tsao
Department of Materials Science and Engineering
National Taiwan University
Taipei 10617, Taiwan
Dr. T.-L. Wu, Prof. C.-H. Cheng
Department of Chemistry
National Tsing Hua University
Hsinchu 30013, Taiwan
The ORCID identification number(s) for the author(s) of this article can be found under https://doi.org/10.1002/adma.201705532.

DOI: 10.1002/adma.201705532

 © 2017 WILEY-VCH Verlag GmbH & Co. KGaA, Weinheim

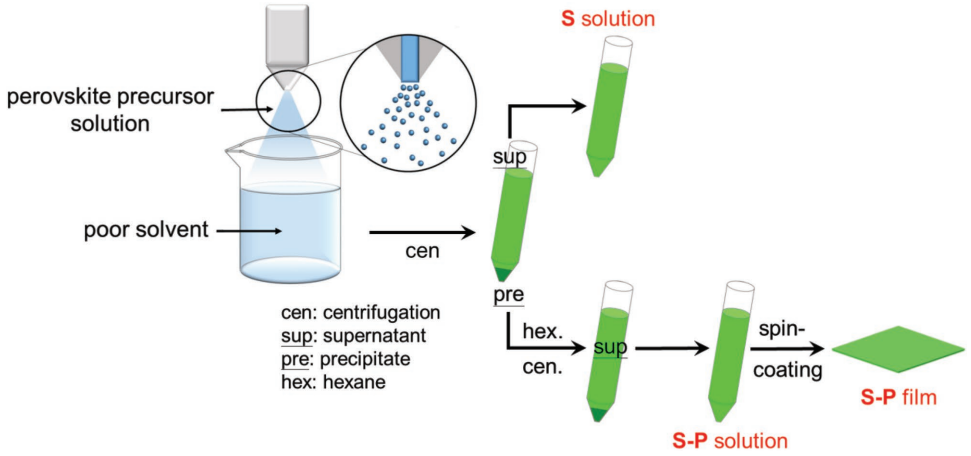

Figure 1. Illustration of the spay-synthesis procedure.

luminance up to 8 500 000 cd m^{-2}. Large-area QD films were integrated on a 5.2 in. organic light emission display (OLED) and demonstrated highly saturated green still images and moving pictures, and conceptually show a wide color gamut up to 119% of the National Television System Committee (NTSC) standard. The films were also used as active emission layers of QD-LEDs, and these devices also showed promising performance, having a preliminary electroluminescent EQE of 1.81%.

Figure 1 illustrates the spray-synthesis procedure, and the traditional drop-synthesis method is shown in Figure S1 in the Supporting Information for comparison. The mixture of organic halide, methylammonium bromide (CH_3NH_3Br, MABr), and lead bromide ($PbBr_2$) with organic ligands (oleic acid and *n*-octylamine) was dissolved in a good solvent, dimethylformamide (DMF), and sprayed into a poor solvent, toluene. Unlike the traditional method, the microsize droplets of the sprayed solution ensure a much larger contact surface area and increased mixing between the precursor-dissolved good solvent and the poor solvent, which facilitates high-quality crystallization of perovskite QDs in the poor solvent. Therefore, the quantum dots immediately formed in the toluene solution. The bright greenish solutions in the upper solution were investigated first, and the precipitates toward the bottom were separated. **Figure 2** shows the absorption (Figure 2a), PL spectra (Figure 2b), and transient PL (Figure 2c) of both the traditional drop-synthesized QDs (**D**) and novel spray-synthesized QDs (**S**) toluene solutions.

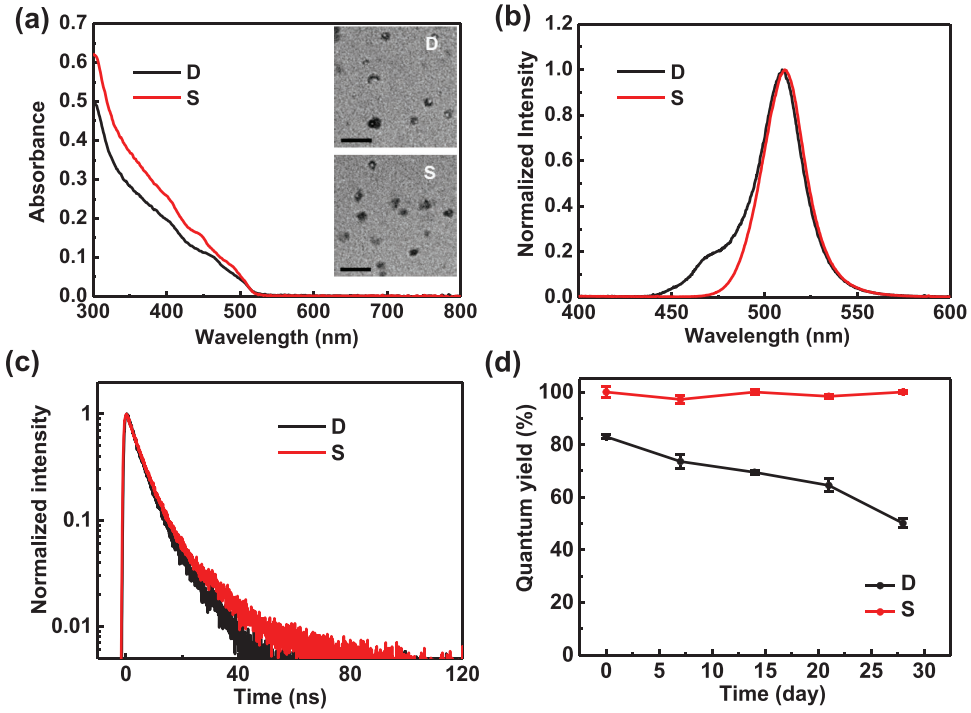

Figure 2. a) Absorption, b) PL spectra, and c) transient PL of the **D** and **S** toluene solutions. Inset of panel (a): the TEM images of the **D** and **S** (scale bar: 50 nm). d) The long-term stability of PLQYs for the **D** and **S** solutions.

© 2017 WILEY-VCH Verlag GmbH & Co. KGaA, Weinheim

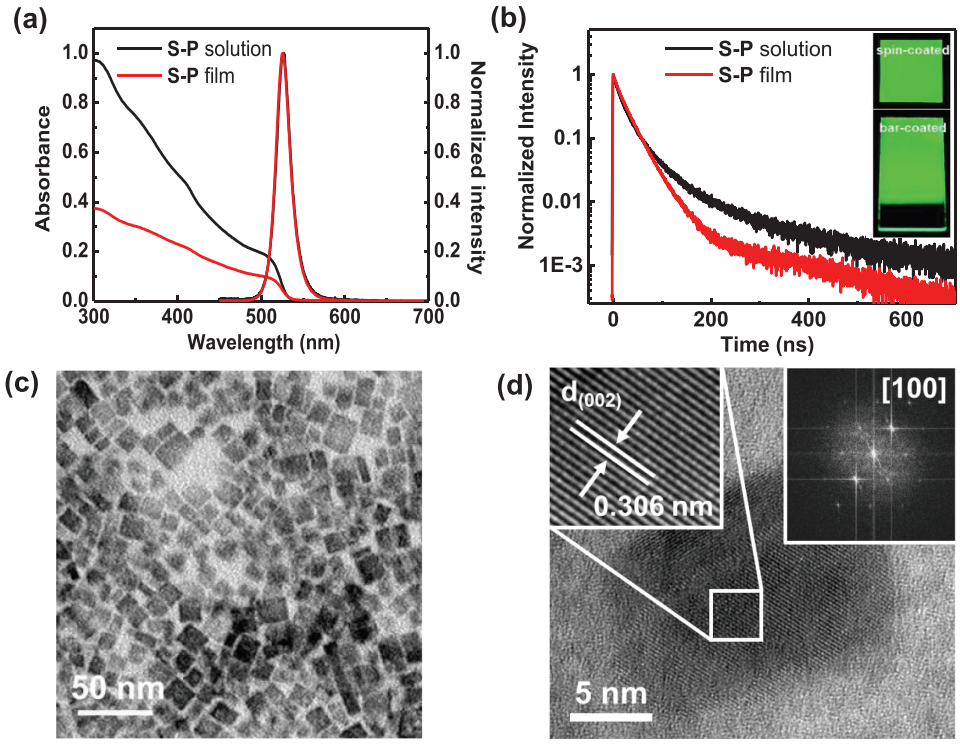

Figure 3. a) Absorption and emission spectra, and b) transient PL of both the **S-P** solution and the **S-P** thin film. Inset of panel (b): the UV light illuminated spin-coated and bar-coated thin films obtained from **S-P** solutions. c) The TEM image of **S-P** showed cubic-shaped QDs with an average size of 14 nm. d) The HR-TEM and the FFT image of the **S-P** QDs.

Their transmission electron microscopy (TEM) images are shown in the inset of Figure 2a. The higher absorption in **S** indicates a higher concentration of QD in the upper solution compared to the **D** counterpart. However, it should be noted that a majority of the QD production occurred and remained in the precipitates in both cases. **S** exhibited Gaussian-shaped PL emission at 511 nm with spectrum FWHM ≈27 nm. **D** showed a similar peak PL emission wavelength of 511 nm but displayed an additional emission peak at ≈470 nm. This additional emission may arise due to the existence of smaller QDs. **D** showed a 6.88 ns PL lifetime and a ≈80% PLQY, which are consistent with the values reported in previous literatures.[19,27] Intriguingly, **S** exhibited a longer PL lifetime of 9.05 ns and a high PLQY of ≈100%. The near-unity PLQY value was apparently 20% higher than that of the QD made with the traditional method. Moreover, a stability test over 1 month in the original toluene solution, as shown in Figure 2d, indicated that **S** was much more stable than **D**, with negligible QY decay over a month for **S** compared to <50% PLQY after a month for **D**. Although the **S** solution exhibited high PLQY and stability, the solutions consisted of hard-to-separate excess oleic acid and were difficult to cast as uniform films. The casted thin film also showed a very low PLQY around 1–2%, which resulted from a high quenching rate in the solid state, presumably due to inferior QD qualities and interference by excess oleic acid contamination.

The precipitates of the **S** solution also showed bright lumination under UV light excitation, which motivated the investigation of their photophysical properties. The precipitates were then resuspended in a hexane solution and surprisingly the solution also exhibited an ≈100% absolute PLQY with a peak emission wavelength of 526 nm and a narrow spectrum FWHM of ≈20 nm. **Figure 3**a–c shows the absorption spectrum, PL spectrum, and time-evolution PL, and TEM image of the re-suspended spray-synthesized precipitates (**S-P**). The lower-magnification TEM image is shown in Figure S2 (Supporting Information). Figure 3d shows the high-resolution TEM (HR-TEM) image and fast Fourier transform (FFT) image of the **S-P** QDs. The selected area electron diffraction (SAED) pattern is shown in Figure S3 (Supporting Information). The HR-TEM image of traditional QD (**D**) is also shown in Figure S4 (Supporting Information) for comparison. Interestingly, **S-P** showed an almost perfect cubic shape with an average size of 14 nm, which was larger than the above-mentioned irregular-sphere-shaped QDs from the upper solutions. The organometallic lead halide QDs usually show an irregular sphere shape and this distinct feature of perfect cubic shape was previously only observed in high-performance Cs-based inorganic perovskite QDs.[19,28] More interestingly, these cubic QDs that we observed showed a much longer PL lifetime of 42.3 ns, which was almost fivefold longer than that of the QDs in the upper solution. The cubic QD solution also exhibited excellent stability and showed no PLQY degradation in 3 months.

We also found that **S-P** solid-state QD neat films can easily be realized by both spin-casting and bar-coating. The UV illuminated bar-coated and spin-coated QD thin films are shown in the inset of Figure 3b. From Figure 3, the QD films showed almost an identical PL emission spectrum compared to the solution (Figure 3a) and an exceptionally long PL lifetime of 33.3 ns with a biexponential decay behavior (Figure 3b). In contrast to traditional organometallic lead halide QDs, which

© 2017 WILEY-VCH Verlag GmbH & Co. KGaA, Weinheim

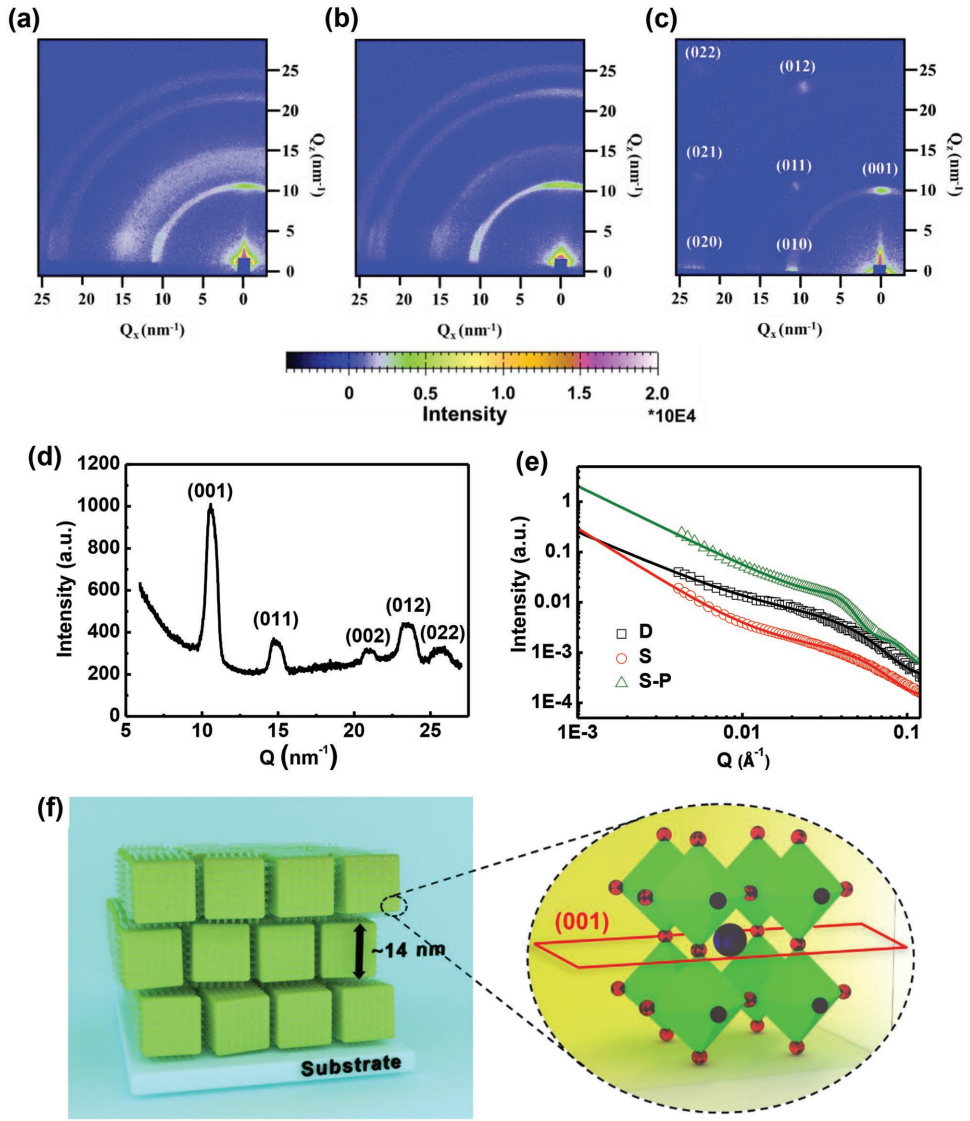

Figure 4. The GIWAXS patterns of the films obtained from a) **D**, b) **S,** and c) **S-P**. d) The ring-averaged GIWAXS profile of the **S-P** film. e) The GISAXS profiles of the corresponding thin films (symbol: experimental data, solid line: fitted curve). f) Illustration of the nanomorphology and crystal orientation of cubic QD thin films.

usually showed much lower PLQY in the solid-state films, the QD films here exhibited extraordinarily high absolute PLQY up to 100%. This high PLQY value of the perovskite solid state is among the highest reported in all kinds of organic and inorganic halide perovskites and has never been observed in the $MAPbBr_3$ films. The long-term PLQY stability of the **S-P** neat film is shown in Figure S5 (Supporting Information). Only a 9% of PLQY decrease was observed in 2 months.

The nanostructure of the QD thin films was investigated by grazing-incidence wide-angle X-ray scattering (GIWAXS) and grazing-incidence small-angle X-ray scattering (GISAXS). The GIWAXS patterns of thin films made from the **D**, **S**, and **S-P** solutions are shown in **Figure 4**. The ring-averaged GIWAXS profile of the **S-P** film is shown in Figure 4d. The GIWAXS pattern of films cast from the **D** and **S** solutions exhibited diffraction rings, which indicates randomness in the orientation of the crystals (QDs) within the films. In contrast, the GIWAXS pattern of the **S-P** film shows a characteristic structure of a near-single crystal. The GIWAXS profile (Figure 4d) displays the diffraction peaks of $MAPbBr_3$ perovskite, which are consistent with X-ray diffraction (XRD) spectra calculated by the single crystal (cubic system; space group: $Pm\bar{3}\ m$, $a = b = c =$ 5.91 Å) and with previously reported structures.[20,29,30] The diffraction peaks of (001), (011), (002), (012), and (022) planes are located at the scattering vector Q = 10.6, 15.0, 21.1, 23.6, and 26.0 nm^{-1}, respectively (corresponding to XRD $2\theta = 15.0°$, 21.2°, 30.2°, 33.9°, and 37.2°, respectively; $Q = 4\pi/\lambda \sin\theta$, where λ is the X-ray wavelength and θ is the scattering angle). The out-of-plane spot for the GIWAXS pattern of the **S-P** film (Figure 4c) reveals that the (001) planes of near-single-crystalline $MAPbBr_3$, with a d-spacing of 5.91 Å, are oriented in parallel to the film substrate. The diffraction spots exhibit a slightly

© 2017 WILEY-VCH Verlag GmbH & Co. KGaA, Weinheim

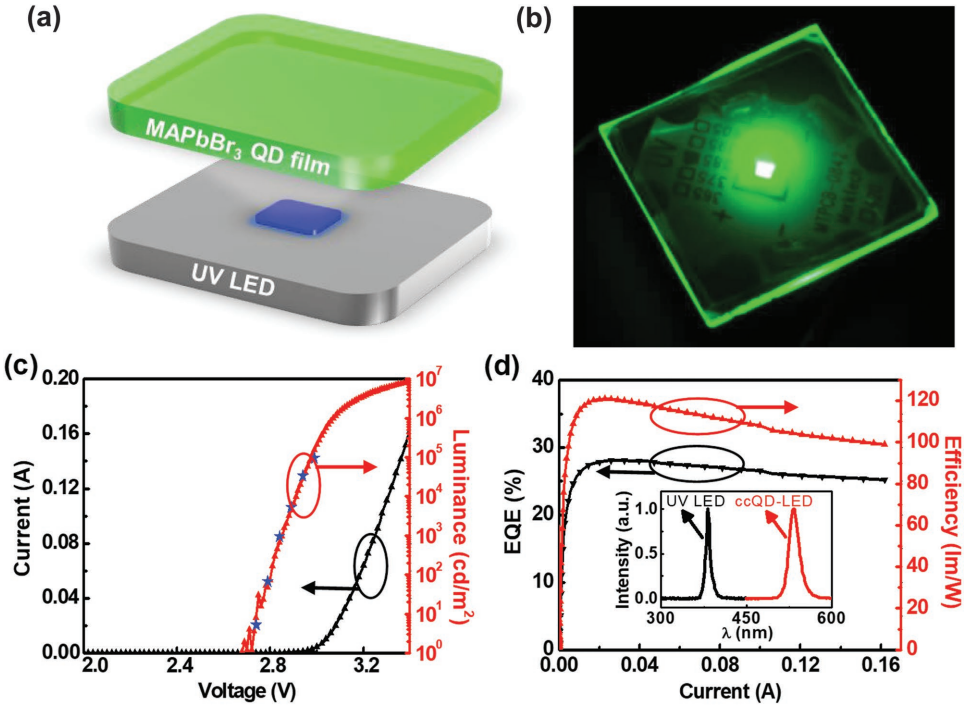

Figure 5. a) Schematic configuration and b) actual image of green emission for the ccQD-LED. c) The current–voltage–luminescence (*I*–*V*–*L*) characteristics of the ccQD-LED. The luminance measured by a spectroradiometer is indicated with a star icon. d) Power efficiency and EQE of the ccQD-LED. Inset: the emission spectra of the UV LED and ccQD-LED.

angular distribution over various directions, indicating the slight misalignment of the orientation between QDs. This well-ordered film possesses the benefits of high crystallinity and high quantum confinement of the excitons.

The GISAXS profiles corresponding to the films investigated by the GIWAXS study are shown in Figure 4e. The GISAXS profiles of the films from **D** and **S** show a typical scattering characteristic without interparticle effect (i.e., no ordering). The form factor model of spherical particles based on the assumption of Schulz size distribution can be adopted and well fitted to the experimental GISAXS intensity profile.[31] The model-determined diameters of QDs in the films from **S** and **D** are 6.2 and 7.1 nm, respectively. The fitted polydispersity values of particles, defined as the ratio of the variance in size distribution to the mean radius, are 0.23 and 0.22 for **S** and **D**, respectively, demonstrating the broadness of the QD size distributions. The GISAXS profile of the **S-P** film shows the scattering peak at Q_m = 0.035 Å^{-1} caused by the interactions between particles (ordering effect). The size of QDs in the film can be roughly estimated to be 18 nm by the simple rule that domain size = $2\pi/Q_m$. The GISAXS profile was well-fitted with the Schulz size distribution model and determined a more accurate mean diameter of QDs, which was 14 nm with very small polydispersity of 0.03. The size range of QDs is consistent with those of cubic QD crystals observed by TEM (Figure 3c; Figure S2, Supporting Information). The schematic representation of the structure and morphology in the film at different scales is shown in Figure 4f. The X-ray photoemission spectroscopy (XPS) results of the **S-P** film are shown in Figure S6 (Supporting Information) and the atomic ratio between Br and Pb is about 70:30.

Encouraged by the excellent PLQYs of **S-P** QD thin films comprising $MAPbBr_3$, we then applied them as color conversion films for optoelectronic applications. **Figure 5** shows the schematic configuration of the color conversion-type QD-LED (ccQD-LED) (Figure 5a) and an image of the actual green emission (Figure 5b). The cubic $MAPbBr_3$ QD thin films were pumped by a commercially available UV LED. The current–voltage–luminescence (*I*–*V*–*L*) characteristics of the ccQD-LED are shown in Figure 5c. High EQE of 28.1% and excellent power efficiency of 121 lm W^{-1} were observed with maximum forward-direction luminescence as high as 8 500 000 cd m^{-2} (Figure 5d). The ccQD-LED showed a saturated green emission with Commission Internationale de I'Eclairage (CIE) 1931 coordinates of (0.161, 0.769) owing to its narrow emission spectrum, having FWHM value down to 20 nm. This green emission is more saturated than standard Red Green Blue, Digital Cinema Initiatives-P3 (DCI-P3), and NTSC standards. The high efficiency, very saturated emission color together with capability of very high brightness of the ccQD-LED all suggest its promising use as a high-brightness backlight with exceptionally high color gamut for current liquid crystal display applications.

The pixelated color conversion was demonstrated utilizing the color conversion type QD-OLED (ccQD-OLED) structure, which is shown in **Figure 6**a. The large area QD film was bar-coated on a thin glass substrate and the substrate was attached onto a consumer cell phone with a 5.2 in. OLED screen. The still image of the demonstration is shown in Figure 6b, and the moving picture videos are included in the Supporting Information. The pixelated still image and moving blue images can be converted by the QD thin films to green images with

© 2017 WILEY-VCH Verlag GmbH & Co. KGaA, Weinheim

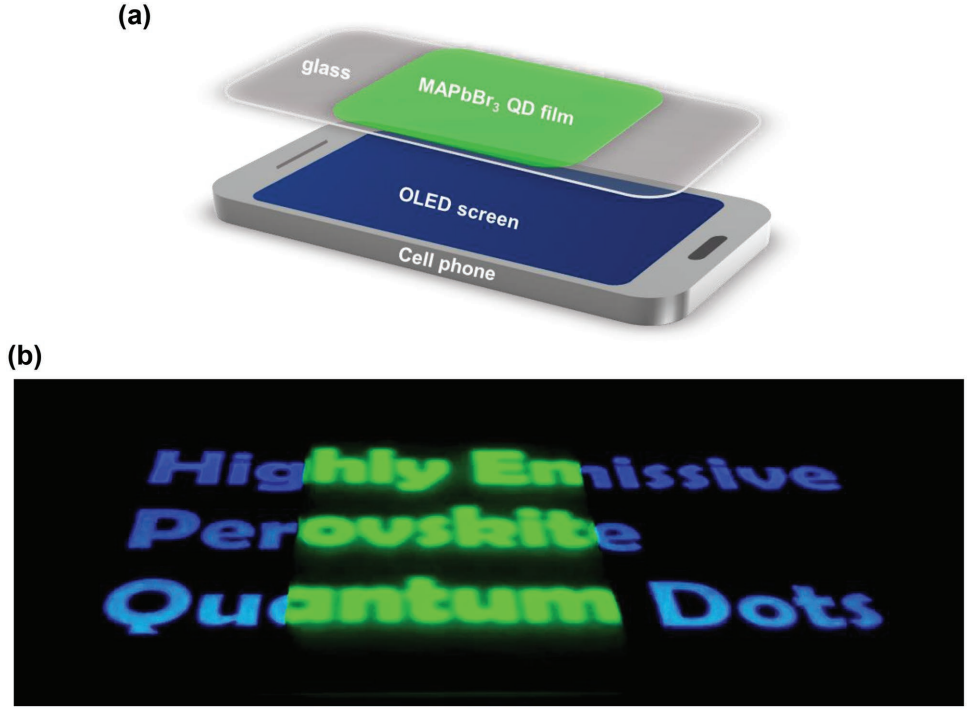

Figure 6. a) Illustration of the hybrid ccQD-OLED display. b) Demonstration of highly saturated images. The movie file of the converted moving pictures is included in the Supporting Information.

a highly saturated color. The results indicate that these thin films can not only be applied in backlight displays, but can also be directly pixelated as a new ccQD-OLED hybrid display. The original emission spectra of red, green, and blue pixels of the OLED are shown in Figure S7a (Supporting Information) and the color gamut is shown in Figure S7b (Supporting Information). The color gamut (black line) displayed a 15% increment due to the very saturated green emission, which corresponds to a 119% NTSC or a 123% DCI-P3 standard.

The QD films were also integrated with organic hole-transporting and electron-transporting layers and behaved as electrically-active emission layer of the LEDs. As shown in Figure S8 (Supporting Information), these electrically active type QD-LEDs (eaQD-LEDs) exhibited an EQE of 1.81%, current efficiency of 7.08 cd A^{-1}, and a maximum luminescence of 735 cd m^{-2}. The moderate performance of these eaQD-LEDs was primarily due to the insulating ligands of the QDs. Recent literature suggests that further modifications of the QD ligands can substantially improve the device performance.[32] The optimization of the device is currently underway and the results will be reported in the future.

We further applied the method to synthesize red- and blue-emitting QDs. The red ones ($CH_3NH_3PbBr_xI_{3-x}$) showed very low PLQYs, possibly due to high sensitivity of oxygen and moisture, and our synthesis method involved inevitable air exposure during the process. The cyan ($CH_3NH_3PbBr_2Cl$) and blue ($CH_3NH_3PbBrCl_2$) ones showed 86% and 52% PLQYs, respectively. The PL spectra are shown in Figure S9 (Supporting Information).

In conclusion, we demonstrate a novel spray method to synthesize highly emissive cubic-shaped QDs composed of organometallic perovskite with an average size of 14 nm. The solution and solid-state PLQYs of these QDs were both near unity. An intriguing near-single-crystal nanomorphology was found by GIWAXS measurement of the QD thin films, which has never been observed in $MAPbBr_3$ thin films, and partially explained the unquenched ≈100% PLQY observed in these solid states. The thin films were then integrated with LEDs and OLEDs. The ccQD-LED hybrid device showed an extremely saturated green emission with CIE coordinates of (0.161, 0.769) and exhibited excellent EQE of 28.1%, power efficiency of 121 lm W^{-1}, and very high brightness of 8 500 000 nits. The ccQD-OLED hybrid display also successfully demonstrated high-definition still images and moving pictures with a 119% NTSC and 123% DCI-P3 color gamut, which corresponds to a 115% enlargement of the original state-of-the-art high color gamut OLED display. Our results indicate that the novel spray-synthesized organometallic halide perovskite QDs are not only scalable, highly stable, and highly emissive even in solid-state neat films, but also widely applicable in ccQD-LED and ccQD-OLED hybrid devices. The stable and highly emissive thin films may also find useful applications in optical-type sensors, bioimaging, and luminescent solar concentrators.

Experimental Section

Synthesis of $CH_3NH_3PbBr_3$ QDs: A vial with 0.8 mmol $PbBr_2$, 0.8 mmol MABr, 0.06 mL *n*-octylamine, and 2 mL oleic acid was co-dissolved in 10 mL DMF to form a clear precursor solution. The precursor solution was moved into the glovebox and was added into a dispenser (SV-6 spray valve with a 2.0 mm nozzle diameter, Musashi Engineering, Inc.) to be dropped (**D**) or sprayed (10 kPa N_2 blowing gas pressure) (**S**) into 50 mL of toluene to produce a yellow–green colloidal solution. The

© 2017 WILEY-VCH Verlag GmbH & Co. KGaA, Weinheim

yellow–green colloidal solution was centrifuged at 6000 rpm for 10 min to separate the upper solutions and the precipitates. The cubic perovskite QD solution (**S-P**) was obtained by resuspending the spray-synthesized precipitates in a hexane solution and centrifuged at 6000 rpm for 20 min to remove the very large particles. The bright supernatant hexane solution was kept for further use.

Fabrication of ccQD-LED Device and ccQD-OLED Display: The S-P solution was spin-coated onto the fused silica substrate at 1000 rpm for 60 s to form the QD film. Then, the QD film was clamped onto an UV LED (MTSM385 UV LED) as a hybrid ccQD-LED device. The ccQD-OLED display was demonstrated by integrating a consumer 5.2 in. OLED screen cell phone with a bar-coated large-area QD film on a glass substrate.

Fabrication of eaQD-LED Device: Indium–tin oxide (ITO)-coated glass substrates were cleaned with detergent and bathed sequentially in deionized water, acetone, and methanol for 15 min each. The clean substrates were treated with UV–ozone for 5 min, and then poly(3,4-ethylenedioxythiophene):poly(styrene sulfonate) (PEDOT:PSS) was spin-coated onto the ITO glass. The PEDOT:PSS layer was baked at a temperature of 135 °C on a hot plate for 30 min. Then, all the substrates were transported into a nitrogen atmosphere glovebox for the deposition of subsequent layers. The hole-transporting layer of poly(9-vinylcarbazole) (PVK) (6 mg mL^{-1} in chlorobenzene) was spin-coated on the PEDOT:PSS layer at 4000 rpm for 60 s then annealed at 110 °C for 0.5 h. The emission layer of $MAPbBr_3$ QDs (25 mg mL^{-1} in *o*-xylene) was then spin-coated onto the PVK layer at 2000 rpm for 60 s, and the substrates were transferred into a high-vacuum evaporation chamber. The electron-transporting layer of 2,2′,2″-(1,3,5-benzinetriyl)-tris(1-phenyl-1-*H*-benzimidazole) (TPBi), electron injection layer of 8-hydroxyquinolinolato-lithium (Liq), and aluminum cathode were deposited by thermal evaporation. The devices were configured as ITO/PEDOT:PSS (40 nm)/PVK (10 nm)/QD neat film (≈30 nm)/TPBi (60 nm)/Liq (2 nm)/Al. The active area of the device, defined as the overlap area of ITO pattern and aluminum cathode, was 1 mm^2.

Characterization and Measurements: TEM images were analyzed with a JEM-2100 transmission electron microscope (accelerating voltage: 200 kV). HR-TEM, FFT, and SAED images were acquired with a JEOL JEM-3000F high-resolution transmission electron microscope (accelerating voltage: 300 kV). XPS spectra were taken with ULVAC-PHI PHI 5000 Versaprobe II electron spectroscopy for chemical analysis. The PL spectra were detected in a front-face configuration by using a fiber-based spectrograph and a charge-coupled device (CCD) camera (PIXIS 256BR, Princeton Instruments), and a stable diode laser (λ = 405 nm) as the pumping source. Absolute PLQY was performed according to the literature[33] and detected by using a calibrated integrating sphere system (Labsphere) equipped with a CCD spectrograph. The detail schematic diagram of the PLQY measurement is shown in Figure S10 (Supporting Information). The uncertainty of the PLQY value was estimated around ±2% owing to the stability of the excitation source and the uncertainty of the radiometric calibration source. The PLQY value was double confirmed by a Rhodamine 6G ethanol solution with a measured PLQY of 95 ± 2%. Absorption spectra were measured by using an ultraviolet–visible spectrophotometer (UV2600, Shimadzu). Transient PL was measured by using a pulsed diode laser (λ = 375 nm, PicoQuant) as an excitation source and a photon-counting photomultiplier tube as a detector. The photon counts were accumulated with a time-correlated single photon counting module (SPC-130-EM, Becker & Hickl GmbH). Simultaneous GIWAXS/GISAXS measurement was performed at BL23 beam line of National Synchrotron Radiation Center, Taiwan. The GIWAXS and GISAXS patterns were simultaneously collected with different 2D detectors during measurement. The energy of the X-ray with an incidence angle of 0.2° was 14 keV. Through the standard calibrations and data reduction procedures, the GISAXS/GIWAXS intensity data were expressed as a function of the scattering vector *Q*. The 1D GISAXS profile was reduced along the in-plane direction (parallel film or substrate surface) of 2D GISAXS patterns.[34] The film specimens for scattering measurement were deposited on the Si substrate with 2 × 2 cm^2. The ccQD-LED hybrid device and esQD-LED device characteristics were measured using a source meter (2363A, Keithley Instruments, Inc.) and a calibrated integrating sphere system (Labsphere), which is illustrated in Figure S11 (Supporting Information). The forward-direction luminesce was detected by a silicon photodetector calibrated by a PR-650 SpectraScan colorimeter (Photo Research, Inc.). The forward-direction luminesce was double confirmed by a spectroradiometer (Konica Minolta CS-2000).

Supporting Information

Supporting Information is available from the Wiley Online Library or from the author.

Acknowledgements

The authors would like to acknowledge the financial support from the Ministry of Science and Technology of Taiwan (Grant Nos. 105-2112-M-007-016-MY3, 105-2628-E-007-008-MY3).

Conflict of Interest

The authors declare no conflict of interest.

Keywords

hybrid devices, perovskite quantum dots, quantum yields, spray synthesis

Received: September 24, 2017
Revised: November 22, 2017
Published online: December 22, 2017

[1] M. M. Lee, J. Teuscher, T. Miyasaka, T. N. Murakami, H. J. Snaith, *Science* **2012**, *338*, 643.
[2] D. Liu, T. L. Kelly, *Nat. Photonics* **2014**, *8*, 133.
[3] W. Nie, H. Tsai, R. Asadpour, J.-C. Blancon, A. J. Neukirch, G. Gupta, J. J. Crochet, M. Chhowalla, S. Tretiak, M. A. Alam, H.-L. Wang, A. D. Mohite, *Science* **2015**, *347*, 522.
[4] Y. H. Kim, H. Cho, J. H. Heo, T. S. Kim, N. Myoung, C. L. Lee, S. H. Im, T. W. Lee, *Adv. Mater.* **2015**, *27*, 1248.
[5] Z. Chen, C. Zhang, X. F. Jiang, M. Liu, R. Xia, T. Shi, D. Chen, Q. Xue, Y. J. Zhao, S. Su, H. L. Yip, Y. Cao, *Adv. Mater.* **2016**, *29*, 1603157.
[6] H. Cho, S.-H. Jeong, M.-H. Park, Y.-H. Kim, C. Wolf, C.-L. Lee, J. H. Heo, A. Sadhanala, N. Myoung, S. Yoo, S. H. Im, R. H. Friend, T.-W. Lee, *Science* **2015**, *350*, 1222.
[7] Z.-K. Tan, R. S. Moghaddam, M. L. Lai, P. Docampo, R. Higler, F. Deschler, M. Price, A. Sadhanala, L. M. Pazos, D. Credgington, F. Hanusch, T. Bein, H. J. Snaith, R. H. Friend, *Nat. Nanotechnol.* **2014**, *9*, 687.
[8] Y.-H. Kim, H. Cho, T.-W. Lee, *Proc. Natl. Acad. Sci. USA* **2016**, *113*, 11694.
[9] J. Byun, H. Cho, C. Wolf, M. Jang, A. Sadhanala, R. H. Friend, H. Yang, T. W. Lee, *Adv. Mater.* **2016**, *28*, 7515.
[10] H. K. Seo, H. Kim, J. Lee, M. H. Park, S. H. Jeong, Y. H. Kim, S. J. Kwon, T. H. Han, S. Yoo, T. W. Lee, *Adv. Mater.* **2017**, *29*, 1605587.
[11] Y.-H. Kim, G.-H. Lee, Y.-T. Kim, C. Wolf, H. J. Yun, W. Kwon, C. G. Park, T. W. Lee, *Nano Energy* **2017**, *38*, 51.
[12] Y.-H. Kim, C. Wolf, Y.-T. Kim, H. Cho, W. Kwon, S. Do, A. Sadhanala, C. G. Park, S.-W. Rhee, S. H. Im, R. H. Friend, T.-W. Lee, *ACS Nano* **2017**, *11*, 6586.

 © 2017 WILEY-VCH Verlag GmbH & Co. KGaA, Weinheim

[13] H. Cho, C. Wolf, J. S. Kim, H. J. Yun, J. S. Bae, H. Kim, J. M. Heo, S. Ahn, T. W. Lee, *Adv. Mater.* **2017**, *29*, 1700579.
[14] G. Xing, N. Mathews, S. S. Lim, N. Yantara, X. Liu, D. Sabba, M. Grätzel, S. Mhaisalkar, T. C. Sum, *Nat. Mater.* **2014**, *13*, 476.
[15] D. Li, H. C. Cheng, Y. Wang, Z. Zhao, G. Wang, H. Wu, Q. He, Y. Huang, X. Duan, *Adv. Mater.* **2017**, *29*, 1601959.
[16] F. Li, C. Ma, H. Wang, W. Hu, W. Yu, A. D. Sheikh, T. Wu, *Nat. Commun.* **2015**, *6*, 8238.
[17] C. Gu, J.-S. Lee, *ACS Nano* **2016**, *10*, 5413.
[18] B. Hwang, J.-S. Lee, *Sci. Rep.* **2017**, *7*, 673.
[19] F. Zhang, H. Zhong, C. Chen, X.-g. Wu, X. Hu, H. Huang, J. Han, B. Zou, Y. Dong, *ACS Nano* **2015**, *9*, 4533.
[20] W. Deng, X. Xu, X. Zhang, Y. Zhang, X. Jin, L. Wang, S. T. Lee, J. Jie, *Adv. Funct. Mater.* **2016**, *26*, 4797.
[21] F. Zhang, S. Huang, P. Wang, X. Chen, S. Zhao, Y. Dong, H. Zhong, *Chem. Mater.* **2017**, *29*, 3793.
[22] Z. Yuan, Y. Shu, Y. Xin, B. Ma, *Chem. Commun.* **2016**, *52*, 3887.
[23] Q. A. Akkerman, V. D'Innocenzo, S. Accornero, A. Scarpellini, A. Petrozza, M. Prato, L. Manna, *J. Am. Chem. Soc.* **2015**, *137*, 10276.
[24] Y. Kim, E. Yassitepe, O. Voznyy, R. Comin, G. Walters, X. Gong, P. Kanjanaboos, A. F. Nogueira, E. H. Sargent, *ACS Appl. Mater. Interfaces* **2015**, *7*, 25007.
[25] L. Mädler, H. K. Kammler, R. Mueller, S. E. Pratsinis, *J. Aerosol Sci.* **2002**, *33*, 369.
[26] X. Yu, T. J. Marks, A. Facchetti, *Nat. Mater.* **2016**, *15*, 383.
[27] J. Xing, F. Yan, Y. Zhao, S. Chen, H. Yu, Q. Zhang, R. Zeng, H. V. Demir, X. Sun, A. Huan, Q. Xiong, *ACS Nano* **2016**, *10*, 6623.
[28] J. Pan, L. N. Quan, Y. Zhao, W. Peng, B. Murali, S. P. Sarmah, M. Yuan, L. Sinatra, N. M. Alyami, J. Liu, E. Yassitepe, Z. Yang, O. Voznyy, R. Comin, M. N. Hedhili, O. F. Mohammed, Z. H. Lu, D. H. Kim, E. H. Sargent, O. M. Bakr, *Adv. Mater.* **2016**, *28*, 8718.
[29] L. C. Schmidt, A. Pertegás, S. González-Carrero, O. Malinkiewicz, S. Agouram, G. Mínguez Espallargas, H. J. Bolink, R. E. Galian, J. Pérez-Prieto, *J. Am. Chem. Soc.* **2014**, *136*, 850.
[30] D. Shi, V. Adinolfi, R. Comin, M. Yuan, E. Alarousu, A. Buin, Y. Chen, S. Hoogland, A. Rothenberger, K. Katsiev, Y. Losovyj, X. Zhang, P. A. Dowben, O. F. Mohammed, E. H. Sargent, O. M. Bakr, *Science* **2015**, *347*, 519.
[31] H.-C. Liao, C.-S. Tsao, T.-H. Lin, M.-H. Jao, C.-M. Chuang, S.-Y. Chang, Y.-C. Huang, Y.-T. Shao, C.-Y. Chen, C.-J. Su, U. S. Jeng, Y.-F. Chen, W.-F. Su, *ACS Nano* **2012**, *6*, 1657.
[32] J. Li, L. Xu, T. Wang, J. Song, J. Chen, J. Xue, Y. Dong, B. Cai, Q. Shan, B. Han, H. Zeng, *Adv. Mater.* **2017**, *29*, 1603885.
[33] J. C. de Mello, H. F. Wittmann, R. H. Friend, *Adv. Mater.* **1997**, *9*, 230.
[34] J. Schlipf, P. Müller-Buschbaum, *Adv. Energy Mater.* **2017**, *7*, 1700131.

© 2017 WILEY-VCH Verlag GmbH & Co. KGaA, Weinheim